Bioresource Technology 395 (2024) 130388

Contents lists available at ScienceDirect

Bioresource Technology

journal homepage: www.elsevier.com/locate/biortech

Electrochemical coverage of reduced graphene oxide layers on sulfur supported by biochar for enhancing performance of Li-S battery

Huaxia Chen [a,*], Bomiao Wang [a], Dianpeng Sui [b], Chongtai Wang [a], Yingjie Hua [a,*]

[a] School of Chemistry and Chemical Engineering of Hainan Normal University, Key Laboratory of Electrochemical Energy Storage and Energy Conversion of Hainan Province, Key Laboratory of Electrochemical Energy Storage and Light Energy Conversion Materials of Haikou City, Haikou 571158, China
[b] Department of Chemistry, College of Science, Northeastern University, Shenyang 110819, China

HIGHLIGHTS

- Carbon fibers and rGO as conductive components supply double transporting paths of electrons.
- rGO as blocking layers inhibits the soluble sulfur diffusing into electrolyte.
- rGO layers as another redepositing places increase the utilization of sulfur.

GRAPHICAL ABSTRACT

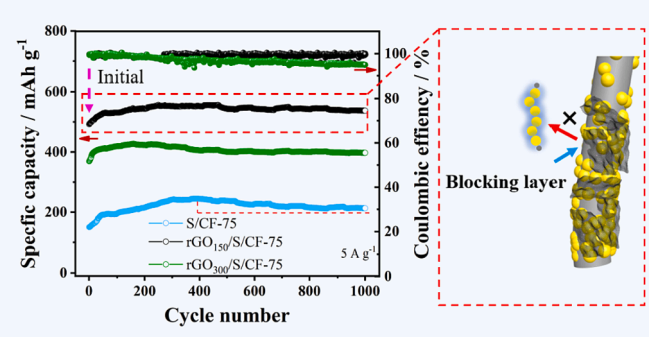

ARTICLE INFO

Keywords:
S/carbon fibers
Reduced graphene oxide
Redistribution of sulfur
Li-S battery

ABSTRACT

To improve the electrochemical performance of Li-S batteries, a cathodic material (rGO_{150}/S/CF-75) was fabricated for Li-S batteries by adopting a melt-flow method to load sulfur on biomass-derived carbon fibers, then the reduced graphene oxide was electrochemically covered on the outside surface of the sulfur. The coverage of reduced graphite oxide layers endows the performance of S/CF-75 multiple improvements. The specific capacity of rGO_{150}/S/CF-75 cathode delivers a specific capacity of 1451.4 mAh g^{-1} at 0.1 A g^{-1}. The specific capacity of rGO_{150}/S/CF-75 cathode can still maintain 537.3 mAh g^{-1} after 1000 cycles at 5 A g^{-1} (109 % capacity retention). The excellent performance of rGO_{150}/S/CF-75 cathode is benefit from not only the conductive paths of reduced graphene oxide layers and protective function of reduced graphene oxide layers inhibiting that the soluble sulfur diffuse into bulk electrolyte, but also the redistribution of sulfur on conductive carbon components during the cycling process.

1. Introduction

With the development of sustainable vehicles driven by electric motors, rechargeable batteries with high energy density and capacity are needed to power the electric engines in the future (Benítez et al., 2022; Canals Casals et al., 2016). Lithium-sulfur battery (LSB) as a

* Corresponding authors.
E-mail addresses: chenhx@hainnu.edu.cn (H. Chen), 521000hua282@sina.com (Y. Hua).

https://doi.org/10.1016/j.biortech.2024.130388
Received 4 December 2023; Received in revised form 9 January 2024; Accepted 24 January 2024
Available online 28 January 2024

promising system possesses a theoretical specific capacity of 1675 mAh g^{-1} and a working voltage of 2.1 V leading to a high theoretical gravimetric energy density of 2552 Wh kg^{-1}, which are greater than those of conventional Lithium-ion battery (Li et al., 2015; Song et al., 2019). In addition, sulfur as active materials have superiorities of natural abundance and environmental benignity. However, sulfur have detrimental characters such as its insulating and soluble natures. Sulfur converts into a short-chain Li_2S/Li_2S_2 and long-chain polysulfides (Li_2S_n, $4 \leq n \leq 8$) during the electrochemical reaction of Li ion with sulfur. The long-chain polysulfides is soluble and can diffuse into electrolyte causing the loss of sulfur from sulfur electrode. Hence, the insulating and soluble natures of sulfur limit the specific capacity, rate capacity and cycling stability of LSB (Cheng & Chung, 2022; Gai et al., 2022; Li et al., 2021b; Lin et al., 2021).

To tackle abovementioned problems, extensive efforts have been devoted to fabrication of cathodic electrode for improving the electrochemical property of LSB. Aiming to conquer the low conductivity of sulfur, carbon materials are usually selected as conductive hosts for loading sulfur to facilitate transportation of electrons (Li et al., 2021a; Phuc et al., 2020; Wu et al., 2020a; Wu et al., 2020b; Xu et al., 2018; Zhao et al., 2022). Biomass-derived carbons have been investigated as potential candidates benefiting from their low cost and sustainability. However, low utilization of sulfur on carbon materials is responsible for hardly approaching theoretical specific capacity of LSB (Xue et al., 2017). Contraposing to issue of the soluble polysulfide, polar metal oxides such as Co_3O_4 (Qiu et al., 2021), Fe_3O_4 (Li et al., 2019), NiO (Zhu et al., 2021), TiO_2 (Yan et al., 2020) and ZnO (Zhang et al., 2020) decorated on carbon can show a strong chemical adsorption with polysulfide by forming O-S band, which can capture the polysulfide for inhibiting the shuttle effects. However, poor electrical conductivity of metal oxide not only restrict the electronic transportations of the electrode, cycling stability and rate-performance of LSB, but also increases the cost of the electrodes (Junhe et al., 2020; Su et al., 2012; Wang et al., 2018). Confronting above problems, a kind of electrode based on complicated strategies has been taken into consideration to apply for LSB such as metal atom-decorated carbon electrode (Gu et al., 2021), heterogeneous/homogeneous electrode (Shi et al., 2022) and atom doping electrode (Ren et al., 2021). These electrodes show the functions of accelerating the redox reaction of polysulfides and chemically trapping polysulfides to improve the cycling stability of LSB. However, these complicated strategies could hardly balance the cost-efficiency and electrochemical property of LSB well (Dong et al., 2021). Hence, practical and facile approaches are urgent to be proposed to fabricate appropriate electrode with both excellent electrical conductivity and fewer losses of sulfur during cycling process to push forward the development of LSB.

Reduced graphene oxide (rGO) exhibits high conductivity to be an additive composite for electrode materials. Besides, the two-dimensional structure of rGO is easy to form conductive layers covering on the insulating sulfur. The coverage of rGO layers could supply channels for efficient transportation of electrons. Significantly, the layers of rGO could also sever as protective layers to inhibit the soluble polysulfides diffusing from inner of electrode into bulk electrolyte during discharging process, which possibly improves the stability of LSB. Based on above strategies, carbon fibers with mechanical robustness are derived from bio-mass material (Tissue), which are engaged as conductive support for loading insulating sulfur by a facile and time-saving melt-flow process. Subsequently, reduced graphene oxide (rGO) was electrochemically covered on sulfur loaded on carbon fibers to form conductive and protective layers as shown in Scheme S1 (see supplementary material). The rGO_{150}/S/CF-75 cathode delivers a superior specific capacity of 1451.4 mAh g^{-1} at 0.1 A g^{-1} among many reported carbon-based cathodes of LSB. Meanwhile, the specific capacity of rGO_{150}/S/CF-75 cathode can maintain in 537.3 mAh g^{-1} after 1000 cycles at 5 A g^{-1}.

2. Experimental section

2.1. Material synthesis

Synthesis of biomass-derived carbon fiber. Tissue (Vinda) was engaged as precursor, which was purchased in local market. First, Tissue was cut into pieces, and then the pieces were transferred into furnace for pre-carbonization at 250 °C for 1 h in atmosphere. After that, the samples continue to calcinate at 300 °C for 1 h and then heated to 700 °C for 1 h in N_2 with the heating rate of 5 °C min^{-1}. Finally, the samples were washed with excessive 10 % HCl and pure H_2O to remove impurities, and the samples dried at 80 °C to obtain carbon fiber denoted as CF.

Loading sulfur on carbon fiber. The sulfur powders were uniformly put on the surface of carbon fiber with different mass ratios of S:CF = 2:1, 3:1 and 4:1, respectively. They were transferred on three pieces of flat glass, and then, put into oil bath and heated to 150 °C for melting sulfur powder until the sulfur could not be observed on the surface of carbon fiber. The samples of S/CF = 2:1, 3:1 and 4:1 were denoted as S/CF-66, S/CF-75 and S/CF-83, respectively.

Synthesis of Reduced graphene oxide-covered carbon fiber with loading of sulfur. Graphene oxide (GO) was prepared from 325 mesh 99.5 % flake graphite powder via the method described in literature (Marcano. et al., 2010), and the concentration of obtained GO is about 5 mg mL^{-1}. The electrochemical coverage of reduced graphene oxide on S/CF-75 was conducted in a two-electrode cell. The electrolyte is 0.01 M Na_2SO_4. The concentration of GO in electrolyte is 0.1 mg mL^{-1}. A piece of graphite foil and S/CF-75 were used as the anode and cathode under a constant current density of 2 mA cm^{-2} for 60 s, 150 s and 300 s, which is denoted as rGO_{60}/S/CF-75, rGO_{150}/S/CF-75 and rGO_{300}/S/CF-75, respectively.

2.2. Material characterization

The microstructure of the samples was characterized by field-emission scanning electron microscopy (FESEM, Hitachi SU8010). Transmission electron microscopy (TEM, JEM-2100) were used to observe the microstructure of the samples. The N_2 adsorption/desorption isotherm (American Micromeritics ASAP 2020) of the samples were recorded at 77.1 K after degassing for 12 h. Thermogravimetric analysis (TGA/DSC3 +) was used to estimate the mass loading of sulfur in S/CF by heating the samples from room temperature up to 300 °C under N_2 with a heating rate of 10 °C min^{-1}. UV–visible spectroscopy (UV, PERSEE T10CS) was used to analyze the electrolytes after long cyclic process.

2.3. Electrochemical characterization

Electrochemical measurements were performed by using coin-type cell (CR2025) assembled in a glove box. The S/CF and rGO/S/CF, acetylene carbon and polyvinylidene fluoride (PVDF) were mixed with a mass ratio of 8:1:1. N-methylpyrrolidone (NMP) was used to form a uniform slurry. The slurry was coated on the aluminum foil by spreader. After being dried, the aluminum foil was cut into disks with diameters of 10 mm, and the disks were pressed at a pressure of 10 MPa for 1 min. The weight of the active material content was about 0.8 ~ 1.0 mg cm^{-2} on the disks. The disk was used as the cathode, the lithium foil was used as the counter electrode, the Celgard 2400 film was used as a separator. Moreover, the 1 M LiTFSI in 1,2-dimethoxy ethane (DME) and 1,3-dioxolane (DOL) (1:1 v/v) were used as the electrolyte. The assembly of the button cell (CR2025) was conducted in the Ar-filled glove box. The cyclic voltammetry (CV) and electrochemical impedance spectroscopy (EIS) were conducted on a CHI 760e electrochemical workstation (Shanghai CH Instrument Company, China). The galvanostatic charging/discharging (GCD) measurement was performed on a Land battery workstation (Wuhan Land Instrument Company, China). All gravimetric capacity was normalized by mass of S.

3. Results and discussion

3.1. Properties of sulfur loaded on carbon fibers

Sulfur is an insulating substance. Carbon is usually engaged as conductive support for loading sulfur when sulfur is used as an electrode. Cellulosic fibers (Tissue) were carbonized into carbon fibers (CF), which can provide a robust substrate for loading sulfur (see supplementary material). This work provides a facile operation called melt-flow method to load sulfur on carbon fibers (see supplementary material). The as-prepared samples are named as S/CF-66, S/CF-75 and S/CF-83, respectively. The 66, 75 and 83 are the mass ratio of sulfur / (carbon fibers + sulfur).

To confirm the structure of S/CF, the as obtained samples were characterized by SEM. Fig. 1**a-c** show the morphologies of S/CF-66, S/CF-75 and S/CF-83. It can be distinguished from morphologies that the aggregation of carbon fibers loads a mass of sulfur with irregular structures. Besides, it can also reflect from elemental distribution of C and S (Fig. 1**d–f**) that the sulfur heterogeneously distributes among carbon fibers. Specifically, much sulfur locate between the carbon fibers, a few sulfur cover on the surface of carbon fibers and some fibers are not covered by sulfur. Compared with CF through TEM images (see supplementary material), S/CF-75 shows dark carbon fibers owning to difficult transmission of electrons from electron gun because of the relative thickness coverage of insulative sulfur on the carbon fibers. Thermogravimetric analysis (TGA) of S/CF-66, S/CF-75 and S/CF-83 was performed in N_2 atmosphere from room temperature to 300 °C (Fig. 1**g**). The weight losses of S/CF-66, S/CF-75 and S/CF-83 are 64.4 wt%, 72.9 wt% and 81.0 wt%, respectively, which generates only a few losses of sulfur comparing with initial addition of sulfur. The weight loss of O in carbon fiber can be ignored, because the carbon fiber is formed in 700 °C. Fig. 1**h** presents the N_2 adsorption/desorption isotherm of CF, which are type-I sorption isotherm curves revealing micropores and mesopores inside of CF. Meanwhile, pore size distribution shows that the mesopores dominates inside of the CF and the specific surface area is 441.6 $m^2\ g^{-1}$. Fig. 1**i** displays the N_2 adsorption/desorption isotherm of CF after loading sulfur (75 %). The micropores almost disappear and the specific surface area of S/CF-75 decreases to 116.6 $m^2\ g^{-1}$ compared with that of CF (441.6 $m^2\ g^{-1}$), which proves that the pores structures in CF are covered or plugged by the sulfur. Based on above characterizations of CF and S/CF, the obtained samples of S/CF contain an amount of sulfur loaded on, between and maybe in carbon fibers, and a part of CF is naked (without coverage of sulfur).

The coin type of LSBs were assembled to investigate the electrochemical performance of S/CF-66, S/CF-75 and S/CF-83, respectively. Fig. 2**a** shows the cyclic voltammetry (CV) curves of S/CF-66, S/CF-75 and S/CF-83 at a scan rate of 0.1 mV s^{-1}. During the cathodic scans, the CV curves of S/CF-66, S/CF-75 and S/CF-83 emerge two reduction peaks, which corresponds to the reduction of S_8 to long-chain polysulfides (Li_2S_n, $4 \leq n \leq 8$) at ~ 2.3 V, and the subsequent transformation from long-chain polysulfides into short-chain of Li_2S_2/Li_2S at ~ 2.06 V. During anodic scans, two overlapped peaks are associated with the transformation of short-chain of Li_2S_2/Li_2S to long-chain polysulfides (Li_2S_n, $4 \leq n \leq 8$) and finally to S_8 (Gaikwad et al., 2021; Huang et al., 2022; Raulo et al., 2021). Among the three CV curves, S/CF-75 exhibits a larger responding current indicating higher utilization of sulfur in S/CF-75 electrode during charging/discharging process. Galvanostatic charging/discharging (GCD) curves of the three electrodes are performed at a current density of 0.1 A g^{-1} in Fig. 2**b**. The GCD curves of the three cathodes show charging/discharging plateaus attributing to the redox reaction of sulfide species. S/CF-75 delivers a superior discharge capacity of 1115 mAh g^{-1} compared with S/CF-66 (788 mAh g^{-1}) and S/CF-83 (661 mAh g^{-1}). The different discharge specific capacities of 1115 mAh g^{-1} (S/CF-75) > 788 mAh g^{-1} (S/CF-66) > 661 mAh g^{-1} (S/CF-83) may be related to the utilization of sulfur. The higher load of sulfur in S/CF-75 could lead to larger contact areas between sulfur, CF, and electrolyte ions compared with S/CF-66 (discharge specific capacity of S/CF-75 > S/CF-66). These contact areas and sulfur in thin film contribute to most specific capacity. The sulfur far away from carbon fiber contribute to less specific capacity owing to its poor conductivity. An excess of sulfur in S/CF-83 may form thicker sulfur on some parts of S/CF-83 which may increase the transportation distance of electrons in

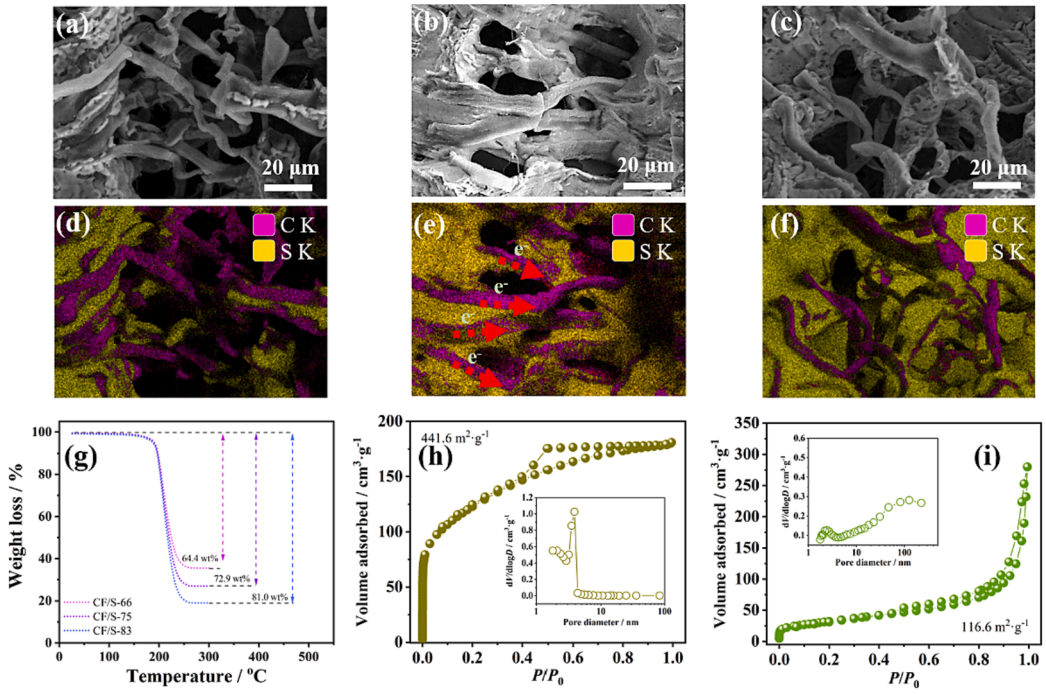

Fig. 1. SEM images of S/CF-66 (a), S/CF-75 (b) and S/CF-83 (c) and corresponding element distribution (d, e and f). (g) TGA curves of S/CF-66, S/CF-75 and S/CF-83 composites. (h) N_2 adsorption/desorption isotherm and pore size distribution (inset) of CF. (i) N_2 adsorption/desorption isotherm and pore size distribution (inset) of S/CF-75.

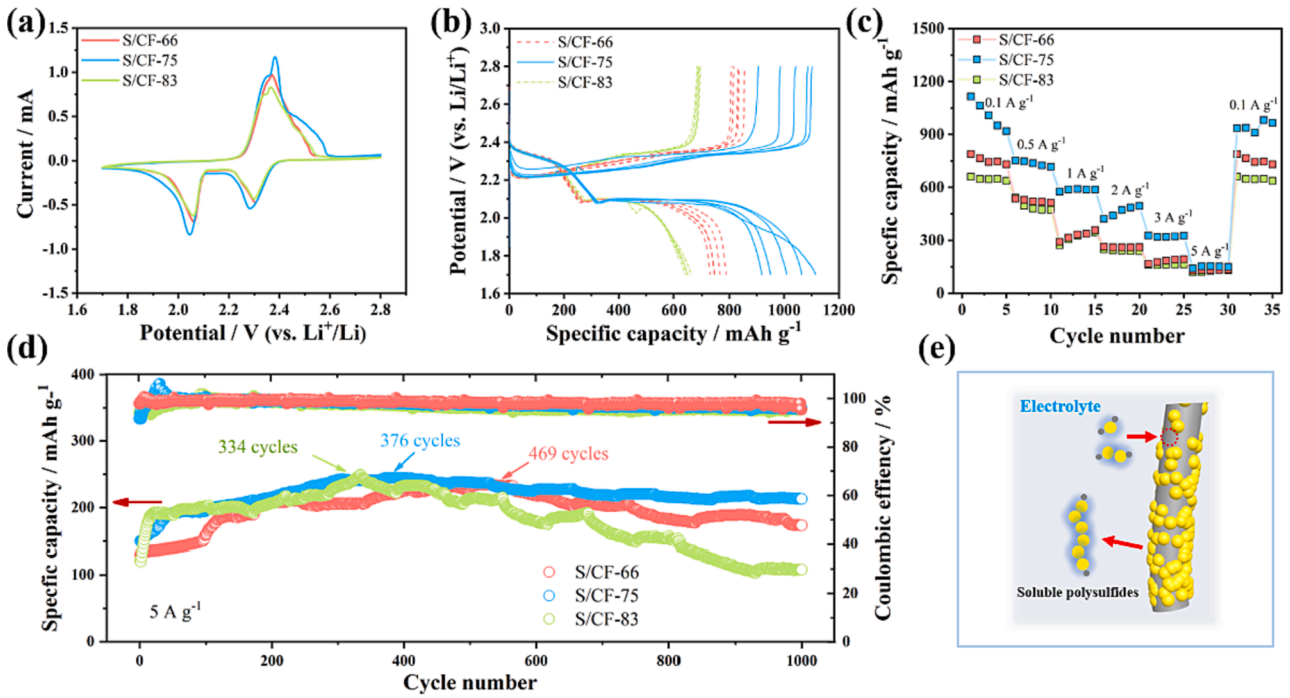

Fig. 2. (a) CV curves of S/CF-66, S/CF-75 and S/CF-83 at 0.1 mV s^{-1}. (b) Charging/discharging curves of S/CF-66, S/CF-75 and S/CF-83 at 0.1 A g^{-1}. (c) Rate performance of S/CF-66, S/CF-75 and S/CF-83 at different current densities. (d) Cycling performance of S/CF-66, S/CF-75 and S/CF-83 at 5 A g^{-1}. (e) Schematic diagram of redistribution of sulfur.

insulating sulfur leading to lower utilization of sulfur. Besides, contact areas between sulfur, CF and electrolyte ion is smaller as shown in Fig. 1**f**. For above reasons, though the sulfur in S/CF-83 is more than those of S/CF-66 and S/CF-75, its specific capacity is smaller than those of S/CF-66 and S/CF-75 due to its lower utilization of sulfur. Fig. 2**c** demonstrates the rate performance of S/CF-66, S/CF-75 and S/CF-83. As the current density increases to 5 A g^{-1}, the specific capacities of S/CF-66, S/CF-75 and S/CF-83 decrease to 129 mAh g^{-1}, 140 mAh g^{-1} and 122 mAh g^{-1}, respectively. The excellent rate capacity of S/CF-75 is attributed to appropriate contact areas and suitable transportation of electrons of S/CF-75 (as above discussions). The cycling stabilities of S/CF-66, S/CF-75 and S/CF-83 cathodes were tested at a high current density of 5 A g^{-1} as shown in Fig. 2**d**. Interestingly, the specific capacities of all the three cathodes deliver a tendency of increasement in the beginning period (up to about 400 cycles) and then decrement to 1000 cycles. S/CF-66, S/CF-75 and S/CF-83 reach the highest specific

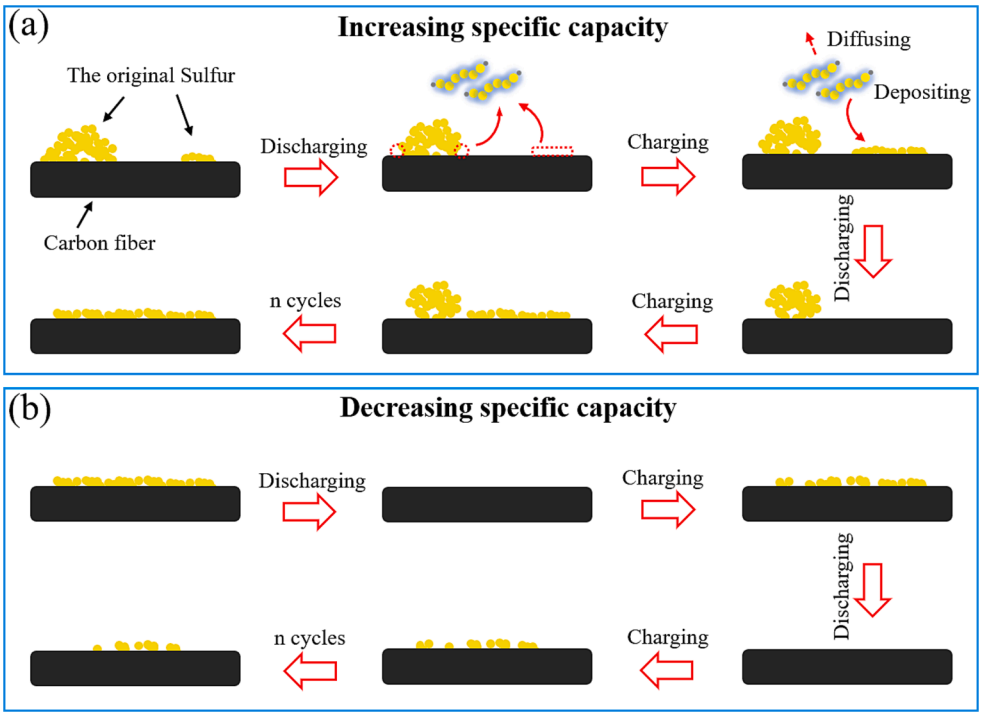

Fig. 3. The schematic diagram of process of increasing specific capacity (a) and decreasing capacity (b) of S/CF-based LSB during cycling process.

capacity (232 mAh g^{-1}) after 469, (244 mAh g^{-1}) 376 and (249 mAh g^{-1}) 334 cycles, respectively. This phenomenon can be ascribed to the redistribution of sulfur during cycling process. The soluble polysulfide from electrode could be divided into two parts which are the block sulfur among or on carbon fibers and the thin film of sulfur covering on the carbon fibers. The block sulfur as the main source of sulfur can dissolve into electrolyte from the contact place with carbon fibers and electrolyte. The thin film of sulfur as another source of sulfur could react with only Li ions and dissolve into in the electrolyte because of the very short transporting distance of electrons in the thin film of sulfur as shown in Fig. 3**a**. In initial discharging process, the soluble sulfur appears and a part of the soluble sulfur diffuses into electrolyte far from the surface of the electrode. Then, during charging process, the soluble polysulfides can redeposit on the naked carbon fibers (surface of conductor) forming a larger area of thin film sulfur compared with the area of thin sulfur in initial state. The larger area of thin film of sulfur leads to higher utilization of sulfur resulting in an increasing specific capacity until the complete conversion of block sulfur into thin film of sulfur (reaching to the highest specific capacity). The highest specific capacities of S/CF-66 (232 mAh g^{-1}), S/CF-75 (244 mAh g^{-1}) and S/CF-83 (249 mAh g^{-1}) exist no significant difference indicating that all the carbon fibers are covered by the thin film of sulfur probably. More sulfur can lead to less cycles to reach the highest specific capacity. Hence, the cycles reaching the highest specific capacity of S/CF-66 (469 cycles) are more than those of S/CF-75 (376 cycles) and S/CF-83 (334 cycles). With the cycling proceeding, the block sulfur is exhausted, or the amount of sulfur dissolving from the block sulfur become smaller than the amount of sulfur diffusing into electrolyte far from the electrode. In this case, the area of the thin film of sulfur on carbon fibers become smaller inducing that the specific capacity decreases as shown in Fig. 3**b**.

3.2. Properties of S/CF covered by reduced graphene oxide

Electrochemical performances show that S/CF-75 cathode with an appropriate load of sulfur exhibits superior electrochemical properties compared with S/CF-66 and S/CF-83 cathodes. Considering the low conductivity and solubility of sulfur species, a rapid electrochemical route was adopted to cover rGO layers on S/CF-75 cathode to investigate if rGO can improve the performance of S/CF-75 because the rGO may serve as conductive layers increasing conductivity of the electrode and blocking layers inhibiting the soluble sulfur diffuses to the electrolyte. The covering process was accomplished in two-electrode system undertaken by galvanostatic technique (2 mA cm^{-2}). In cell system, graphite and S/CF-75 were used as anode and cathode, respectively. 0.01 M Na_2SO_4 sever as supporting electrolyte containing 0.1 mg mL^{-1} GO as source of rGO as shown in Fig. 4**a**. Previous reports proved that electrochemical approaches are able to produce rGO on electrode surface(Toh et al., 2014). In the process of electrochemical reduction, the oxygen-containing functional groups (C = O, O-H and C-O-C) could accept electrons, yielding rGO that attaches on electrode surface(Chen et al., 2011; Guo et al., 2009; Hilder et al., 2011), as illustrated in schematic diagram Fig. 4**b**.

During electrochemical coverage process, coverage time is an important parameter, which could affect the thickness of rGO layer. Three electrochemical coverage times (60 s, 150 s and 300 s) are chosen to observe the effects of rGO layers on S/CF-75 electrode, which is denoted as rGO_{60}/S/CF-75, rGO_{150}/S/CF-75 and rGO_{300}/S/CF-75, respectively. With the lasting of electrochemical coverage time, the gaps on the surface of rGO become less and less suggesting thicker coverage layers of rGO on sulfur and carbon fibers of rGO_{300}/S/CF-75 compared with rGO_{60}/S/CF-75 and rGO_{150}/S/CF-75 as shown in Fig. 5**b**, **d** and **f**. To clarify the function of rGO layers, electrochemical tests were ulteriorly performed in coin cell configurations, and electrochemical results of S/CF-75 are still discussed in this section for comparisons.

Fig. 6**a** shows the comparison of CV curves of S/CF-75, rGO_{60}/S/CF-75, rGO_{150}/S/CF-75 and rGO_{300}/S/CF-75. The potentials of oxidative/reductive peaks of rGO_{60}/S/CF-75, rGO_{150}/S/CF-75 and rGO_{300}/S/CF-75 match well with that of S/CF-75 demonstrating that electrochemical coverage of rGO layers makes no impact on the electrochemical reactions on the electrodes. The responding current of the rGO_{60}/S/CF-75 differs little from that of S/CF-75 indicating that the connected rGO layers do not form after a short electrodeposition time, which also can reflect from the SEM images (Fig. 5**a**). Hence, rGO_{60}/S/CF-75 is ignored in the following discussions. The responding peak currents of rGO_{150}/S/CF-75 and rGO_{300}/S/CF-75 are larger than that of S/CF-75 during redox process implying that the utilization of sulfur increases owing to the improvement of electrical conductivity of S/CF-75 by the rGO layers, because the rGO layers contact on the surface of sulfur supplying another smooth path for electron transportation. The diameter of semicircle (Nyquist plot) represents the charge transfer resistance (R_{ct}) as shown in Fig. 6**e**. The smaller diameters of semicircles of rGO_{150}/S/CF-75 and rGO_{300}/S/CF-75 indicating the improved electrical conductivities originating from rGO layers compared with that of S/CF-75. As a result, more excellent electrical conductivity and higher utilization of sulfur guarantee enhanced specific capacities of rGO_{150}/S/CF-75 (1451.4 mAh g^{-1}) and rGO_{300}/S/CF-75 (1374.5 mAh g^{-1}) at 0.1 A g^{-1} compared with the specific capacity of S/CF-75 (1115 mAh g^{-1}) as shown in Fig. 6**b**. The specific capacity of rGO_{150}/S/CF-75 is higher than that of rGO_{300}/S/CF-75 indicating that the thicker rGO layer (less gaps) may block the Li ion diffuse into the surface of sulfur as shown in Fig. 6**d**. In addition, thicker rGO layers lead to poorer conductivity also limiting the specific capacity of rGO_{300}/S/CF-75. The rGO_{150}/S/CF-75 and rGO_{300}/S/CF-75 exhibit excellent rate capability with gradually increasing current density as shown in Fig. 6**c**. At the current density of 5 A g^{-1}, the specific capacities of rGO_{150}/S/CF-75, rGO_{300}/S/CF-75 and S/CF-75 are 485.9 mAh g^{-1}, 381 mAh g^{-1} and 140 mAh g^{-1},

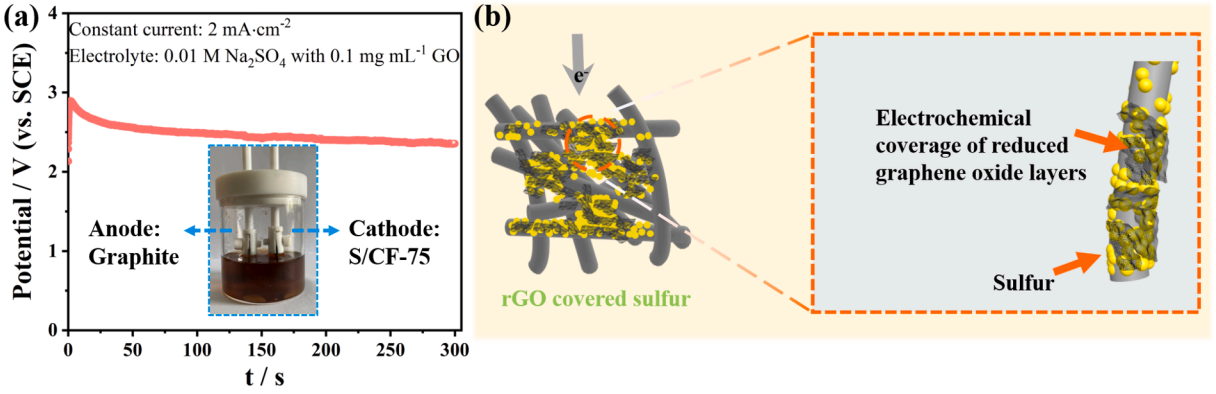

Fig. 4. (a) Electrochemical reduction of graphene oxide on S/CF-75 at a constant current of 2 mA cm^{-2} using two-electrode cell. (b) Schematic illustration of electrochemical coverage of rGO on S/CF-75.

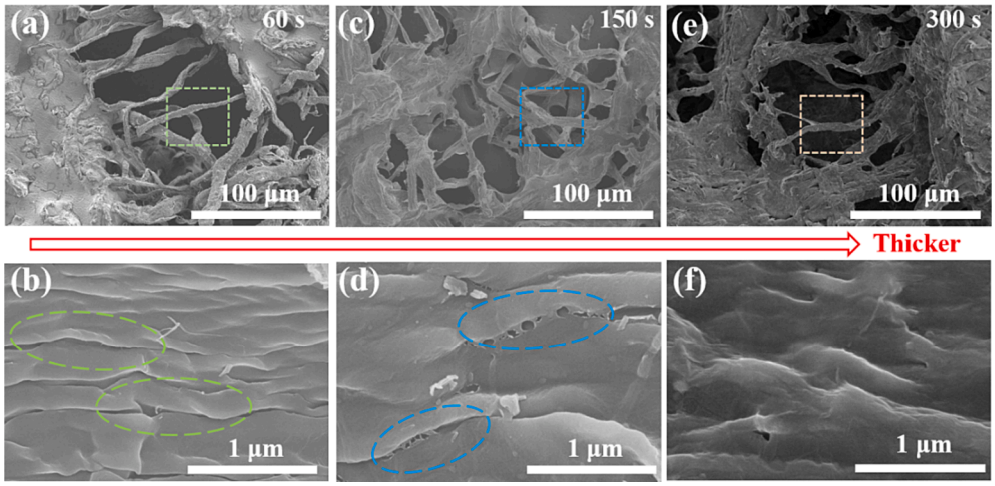

Fig. 5. (a) SEM image of rGO_{60}/S/CF-75. (b) Magnification image of rGO_{60}/S/CF-75. (c) SEM image of rGO_{150}/S/CF-75. (d) Magnification image of rGO_{150}/S/CF-75. (e) SEM image of rGO_{300}/S/CF-75. (f) Magnification image of rGO_{300}/S/CF-75.

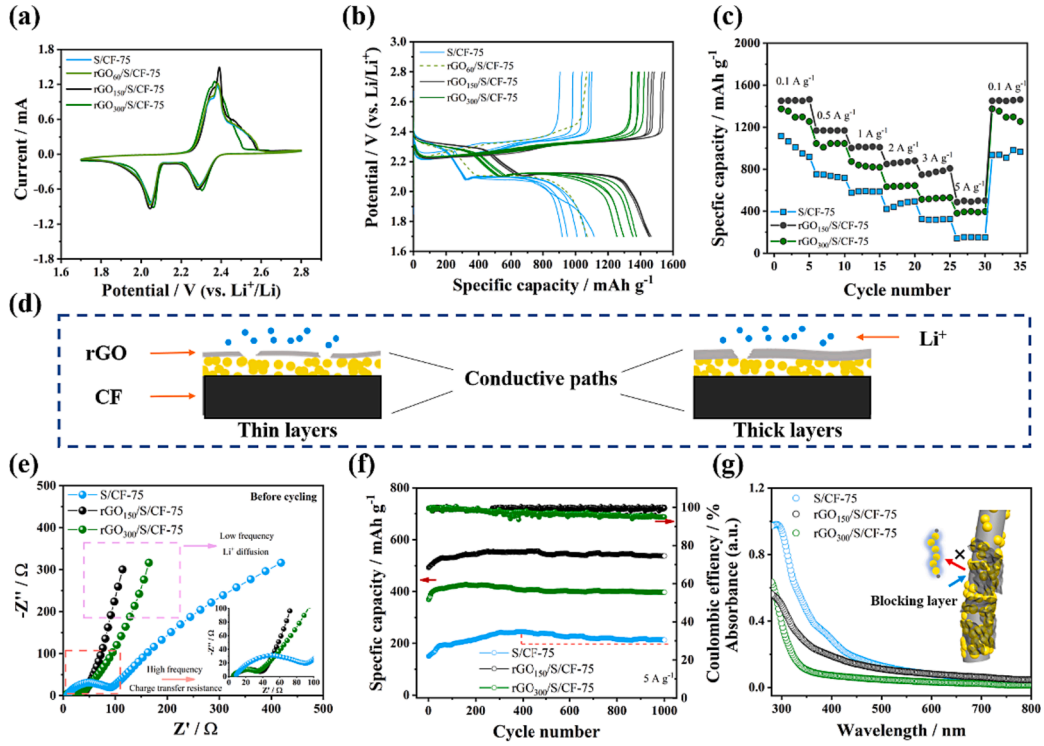

Fig. 6. (a) CV curves of S/CF-75, rGO_{60}/S/CF-75, rGO_{150}/S/CF-75 and rGO_{300}/S/CF-75. (b) GCD curves of S/CF-75, rGO_{60}/S/CF-75, rGO_{150}/S/CF-75 and rGO_{300}/S/CF-75 at 0.1 A g^{-1}. (c) Rate performance of S/CF-75, rGO_{150}/S/CF-75 and rGO_{300}/S/CF-75 at different current densities. (d) The schematic diagram of thin and thick rGO layers. (e) EIS of S/CF-75, rGO_{150}/S/CF-75 and rGO_{300}/S/CF-75 before cycling. (f) Cycling stability of S/CF-75, rGO_{150}/S/CF-75 and rGO_{300}/S/CF-75 at 5 A g^{-1}. (g) UV–vis absorption of polysulfides in the electrolyte from S/CF-75, rGO_{150}/S/CF-75 and rGO_{300}/S/CF-75-based LSB after long-term cycles.

respectively. The excellent rate capacity of rGO_{150}/S/CF-75 is benefiting from the fast transportation of electrons through both rGO layers and carbon fibers. Cycling stability of rGO/S/CF-75 achieves increased retention of 109 % (for rGO_{150}/S/CF-75, from initial 492.0 mAh g^{-1} to final 537.3 mAh g^{-1}) and 108 % (for rGO_{300}/S/CF-75, from initial 369.0 mAh g^{-1} to final 397.2 mAh g^{-1}) after 1000 cycles at 5 A g^{-1} (Fig. 6**f**). The increased specific capacities are also attributed to the redistribution of sulfur, which are similar to the redeposition of sulfur in S/CF-75 during cycling. The difference is that the surface of rGO layers may also be places for redeposition of sulfur. However, rGO_{150}/S/CF-75 and rGO_{300}/S/CF-75 maintain flat platforms of specific capacities after reaching the maximal specific capacities compared with S/CF-75. The flat platforms could originate from the protective function of rGO layers, which can inhibit soluble polysulfide diffusing into bulk electrolyte as well as possible. As a result, the soluble polysulfide is mostly confined to a narrow space forming by the inner surface of rGO and the surface of sulfur or carbon fibers in a complete cycling process, which ensure an excellent cycling stability of rGO_{150}/S/CF-75 and rGO_{300}/S/CF-75, as illustrated in the schematic diagram inside of Fig. 6**g**. Because of the excellent conductivity of rGO, the inner surface of rGO may become another place redepositing sulfur, which could increase the surface of sulfur film improving the utilization of sulfur. Additionally, the outer surface of rGO may contribute a small part of the specific capacity through deposition of sulfur, which diffuses from inside of the electrode

into the bulk electrolyte, on it. That may be the reasons why the specific capacities of rGO_{150}/S/CF-75 and rGO_{300}/S/CF-75 are significantly larger and more stable than that of S/CF-75. The platform of rGO_{300}/S/CF-75 seems flatter than that of rGO_{150}/S/CF-75 indicating that the thicker rGO layers with less gaps on rGO_{300}/S/CF-75 exhibit stronger protection for soluble sulfur, but the specific capacity is limited by the sluggish diffusion of ions because of less gaps on the thicker rGO layers. The speculation can be proved by UV–vis absorption of electrolyte from the batteries based on S/CF-75, rGO_{150}/S/CF-75 and rGO_{300}/S/CF-75 after cycling as shown in Fig. 6**g**. UV–vis absorption of electrolyte from S/CF-75-based battery shows strongest absorption comparing with those from rGO_{150}/S/CF-75 and rGO_{300}/S/CF-75-based batteries. The stronger absorption indicates more soluble polysulfide in the electrolyte of S/CF-75-based battery. The color of the electrolyte from S/CF-75-based battery became yellow after cycling also indicating the more loss of sulfur from the electrode. The colors of the electrolytes from rGO_{150}/S/CF-75 and rGO_{300}/S/CF-75-based battery are almost transparent indicating the blocking function of rGO layers (see supplementary material) (Zhang et al., 2019; Zhong et al., 2019). Electrochemical impedance spectroscopy (EIS) is used to analyze the resistance of S/CF-75, rGO_{150}/S/CF-75 and rGO_{300}/S/CF-75 after cycling (see supplementary material). Two semicircles represent surface film (forming during electrochemical cycles) and charge transfer (Bredar et al., 2020), respectively. Here, the semicircles (charge transfer resistance) of rGO_{150}/S/CF-75 and rGO_{300}/S/CF-75 with smaller diameters manifest that the rGO layers work as conductive component in cycling process. From analysis of electrochemical comparisons, rGO_{150}/S/CF-75 cathode stands out because of suitable load of sulfur, appropriate thickness of rGO layers and connected coverage of rGO layers.

4. Conclusions

The rGO_{150}/S/CF-75-based LSB exhibit a high specific capacity and cycling stability. The excellent performance of rGO_{150}/S/CF-75 cathode is attributed to three effects of the rGO layers. As conductive component, the rGO becomes another transporting path for electrons improving the conductivity of the electrode. As protective layers, the rGO inhibits the soluble sulfur diffusing into bulk electrolyte enhancing cycling stability of the LSB. And as redepositing place, the rGO increases the area of sulfur in thin film raising the utilization of sulfur. This work provides a facile and efficient way to synthesize the S/carbon-based cathode for LSB.

Author contributions

Huaxia Chen: Design and complete experiments, Process experiment data, Draw the figure, Write the manuscript. Bomiao Wang: Conduct SEM characterization of materials and analysis. Dianpeng Sui: Writing, editing, and interpretation of data and the results. Chongtai Wang and Yingjie Hua: Funding acquisition and Project administration.

CRediT authorship contribution statement

Huaxia Chen: Writing – review & editing, Writing – original draft, Conceptualization. **Bomiao Wang:** Software. **Dianpeng Sui:** Writing – review & editing. **Chongtai Wang:** Funding acquisition. **Yingjie Hua:** Funding acquisition.

Declaration of competing interest

The authors declare that they have no known competing financial interests or personal relationships that could have appeared to influence the work reported in this paper.

Data availability

Data will be made available on request.

Acknowledgements

This work was supported by the Hainan Normal University Student Innovation and Entrepreneurship Open Fund (Banyan Tree Fund) (RSYH20231165815X) and the Grants for the Innovation Center of Academician Sun Shigang's Team in Hainan Province.

Appendix A. Supplementary data

Supplementary data to this article can be found online at https://doi.org/10.1016/j.biortech.2024.130388.

References

Benítez, A., Amaro-Gahete, J., Chien, Y.-C., Caballero, Á., Morales, J., Brandell, D., 2022. Recent advances in lithium-sulfur batteries using biomass-derived carbons as sulfur host. Renew. Sust. Energ. Rev. 154, 111783.
Bredar, A.R.C., Chown, A.L., Burton, A.R., Farnum, B.H., 2020. Electrochemical impedance spectroscopy of metal oxide electrodes for energy applications. ACS Appl. Energy Mater. 3 (1), 66–98.
Canals Casals, L., Martinez-Laserna, E., Amante García, B., Nieto, N., 2016. Sustainability analysis of the electric vehicle use in Europe for CO_2 emissions reduction. J. Clean. Prod. 127, 425–437.
Chen, L., Tang, Y., Wang, K., Liu, C., Luo, S., 2011. Direct electrodeposition of reduced graphene oxide on glassy carbon electrode and its electrochemical application. Electrochem. Commun. 13 (2), 133–137.
Cheng, C.S., Chung, S.H., 2022. Nickel-plated sulfur nanocomposites for electrochemically stable high-loading sulfur cathodes in a lean-electrolyte lithium-sulfur cell. Chem. Eng. J. 429, 132257.
Dong, Y., Li, T., Cai, D., Yang, S., Zhou, X., Nie, H., Yang, Z., 2021. Progress and prospect of organic electrocatalysts in Lithium-Sulfur batteries. Front. Chem. 9, 703354.
Gai, L., Zhao, C., Zhang, Y., Hu, Z., Shen, Q., 2022. Constructing a multifunctional mesoporous composite of metallic cobalt nanoparticles and nitrogen-doped reduced graphene oxides for high-performance lithium–sulfur batteries. Carbon Energ. 4 (2), 142–154.
Gaikwad, M.M., Sarode, K.K., Pathak, A.D., Sharma, C.S., 2021. Ultrahigh rate and high-performance lithium-sulfur batteries with resorcinol-formaldehyde xerogel derived highly porous carbon matrix as sulfur cathode host. Chem. Eng. J. 425, 131521.
Gu, X., Deng, L., Ren, X., 2021. Metal atom-decorated carbon nanomaterials for enhancing Li-S/Se batteries performances: A mini review. Front. Energy Res. 9, 626596.
Guo, H.L., Wang, X.F., Qian, Q.Y., Wang, F.B., Xia, X.H., 2009. A green approach to the synthesis of graphene nanosheets. ACS Nano 3 (9), 2653–2659.
Hilder, M., Winther Jensen, B., Li, D., Forsyth, M., MacFarlane, D.R., 2011. Direct electro-deposition of graphene from aqueous suspensions. Phys. Chem. Chem. Phys. 13 (20), 9187–9193.
Huang, B.S., Tu, W.J., Chen, J.S., 2022. Investigation of polysulfide dissolution behavior using various amine groups functionalized order mesoporous carbon as sulfur hosts in lithium-sulfur batteries. Diam. Relat. Mater. 122, 108823.
Junhe, Y., Pan, H.A.N., Yuepeng, P., Fei, D., Shiyou, Z., 2020. Research progress on nanostructured metal oxides as anode materials for Li-ion battery. J. Inorg. Mater. 35 (12), 1295.
Li, G.C., Jing, H.K., Su, Z., Lai, C., Chen, L., Yuan, C.C., Li, H.H., Liu, L., 2015. Hydrophilic separator for high performance lithium sulfur batteries. J. Mater. Chem. A 3 (20), 11014–11020.
Li, J., Niu, Z., Guo, C., Li, M., Bao, W., 2021b. Catalyzing the polysulfide conversion for promoting lithium sulfur battery performances: A review. J. Energ. Chem. 54, 434–451.
Li, H., Shao, F., Wen, X., Ding, Y., Zhou, C., Zhang, Y., Wei, H., Hu, N., 2021a. Graphene/MXene fibers-enveloped sulfur cathodes for high-performance Li-S batteries. Electrochim. Acta 371, 137838.
Li, B., Sun, Z., Zhao, Y., Zhang, Z., 2019. Facile synthesis of three-dimensional carbon nanotube/Fe_3O_4 microspheres as sulfur host for high performance lithium-sulfur batteries. Mater. Lett. 255, 126529.
Lin, Y., Huang, S., Zhong, L., Wang, S., Han, D., Ren, S., Xiao, M., Meng, Y., 2021. Organic liquid electrolytes in Li-S batteries: actualities and perspectives. Energy Storage Mater. 34, 128–147.
Marcano, D.C., Kosynkin, D.V., Berlin, J.M., Sinitskii, A., Zhengzong, S., Slesarev, A., Alemany, L.B., Lu, W., Tour, J.M., 2010. Improved synthesis of graphene oxide. ACS Nano 4 (8), 4806–4814.
Phuc, N.H.H., Takaki, M., Muto, H., Reiko, M., Kazuhiro, H., Matsuda, A., 2020. Sulfur–carbon nano fiber composite solid electrolyte for all-solid-state Li–S batteries. ACS Appl. Energy Mater. 3 (2), 1569–1573.
Qiu, W., Li, J., Zhang, Y., Kalimuldina, G., Bakenov, Z., 2021. Carbon nanotubes assembled on porous TiO_2 matrix doped with Co_3O_4 as sulfur host for lithium-sulfur batteries. Nanotechnology 32 (7), 075403.

Raulo, A., Gupta, A., Srivastava, R., Nandan, B., 2021. Cotton cloth templated in situ encapsulation of sulfur into carbon fibers for lithium-sulfur batteries. Chem. Commun. 57 (4), 544–547.
Ren, X., Liu, Z., Zhang, M., Li, D., Yuan, S., Lu, C., 2021. Review of cathode in advanced Li−S batteries: The effect of doping atoms at micro levels. ChemElectroChem 8 (18), 3457–3471.
Shi, Z., Ding, Y., Zhang, Q., Sun, J., 2022. Electrocatalyst modulation toward bidirectional sulfur redox in Li–S batteries: From strategic probing to mechanistic understanding. Adv. Energy Mater. 12 (29), 2201056.
Song, Y., Cai, W., Kong, L., Cai, J., Zhang, Q., Sun, J., 2019. Rationalizing electrocatalysis of Li–S chemistry by mediator design: progress and prospects. Adv. Energy Mater. 10 (11), 1901075.
Su, Y., Li, S., Wu, D., Zhang, F., Liang, H., Gao, P., Cheng, C., Feng, X., 2012. Two-dimensional carbon-coated graphene/metal oxide hybrids for enhanced lithium storage. ACS Nano 6 (9), 8349–8356.
Toh, S.Y., Loh, K.S., Kamarudin, S.K., Daud, W.R.W., 2014. Graphene production via electrochemical reduction of graphene oxide: Synthesis and characterisation. Chem. Eng. J. 251, 422–434.
Wang, Q., Shang, M., Zhang, Y., Yang, Y., Wang, Y., 2018. Rate-limiting step in batteries with metal oxides as the energy materials. ACS Appl. Mater. Interfaces 10 (8), 7162–7170.
Wu, J., Dai, Y., Pan, Z., Huo, D., Wang, T., Zhang, H., Hu, J., Yan, S., 2020a. Co_3O_4 hollow microspheres on polypyrrole nanotubes network enabling long-term cyclability sulfur cathode. Appl. Surf. Sci. 510, 145529.
Wu, J., Pan, Z., Dai, Y., Wang, T., Zhang, H., Yan, S., Xu, J., Song, K., 2020b. Encapsulation of sulfur cathodes by sericin-derived carbon/Co_3O_4 hollow microspheres for the long-term cyclability of lithium-sulfur batteries. J. Alloy. Compound. 823, 153912.
Xu, J., Zhang, W., Chen, Y., Fan, H., Su, D., Wang, G., 2018. MOF-derived porous N-Co3O4@N–C nanododecahedra wrapped with reduced graphene oxide as a high capacity cathode for lithium–sulfur batteries. J. Mater. Chem. A 6 (6), 2797–2807.
Xue, W., Miao, L., Qie, L., Wang, C., Li, S., Wang, J., Li, J., 2017. Gravimetric and volumetric energy densities of lithium-sulfur batteries. Curr. Opin. Electrochem. 6 (1), 92–99.
Yan, C., Zhou, X., Wei, Y., He, S., 2020. A waste newspaper/multi-walled carbon nanotube/TiO_2 interlayer for improving the cycling stability of lithium-sulfur batteries by anchoring polysulfides. Dalton t. 49 (33), 11675–11681.
Zhang, Z., Yi, Z., Liu, L., Yang, J., Zhang, C., Pan, X., Chi, F., 2020. 3D hollow rGO microsphere decorated with ZnO nanoparticles as efficient sulfur host for high-performance Li-S battery. Nanomaterials 10 (9), 1633.
Zhang, J., You, C., Wang, J., Guo, S., Zhang, W., Yang, R., Fu, P., 2019. Synergistic catalytic effect of ion tunnels with polar dopants to boost the electrochemical kinetics for high-performance sulfur cathodes. ChemElectroChem 6 (19), 5051–5059.
Zhao, T., Chen, J., Dai, K., Zhang, J., Yuan, M., Li, X., Zhang, K., Zhang, J., Li, Y., Liu, Z., He, H., Li, B., Zhang, G., 2022. Boosted polysulfides regulation by iron carbide nanoparticles-embedded porous biomass-derived carbon toward superior lithium-sulfur batteries. J. Colloid Interface Sci. 605, 129–137.
Zhong, M.E., Guan, J., Sun, J., Guo, H., Xiao, Z., Zhou, N., Gui, Q., Gong, D., 2019. Carbon nanodot-decorated alveolate N, O, S tridoped hierarchical porous carbon as efficient electrocatalysis of polysulfide conversion for lithium-sulfur batteries. Electrochim. Acta 299, 600–609.
Zhu, M., Wu, J., Li, S., Luo, X., Zhang, B., Jiang, M., Xu, X., Sheng, W., Xu, J., Song, K., 2021. Flower-like Ni/NiO microspheres decorated by sericin-derived carbon for high-rate lithium-sulfur batteries. Ionics 27 (12), 5137–5145.